Cell Reports

Lactate Limits T Cell Proliferation via the NAD(H) Redox State

Graphical Abstract

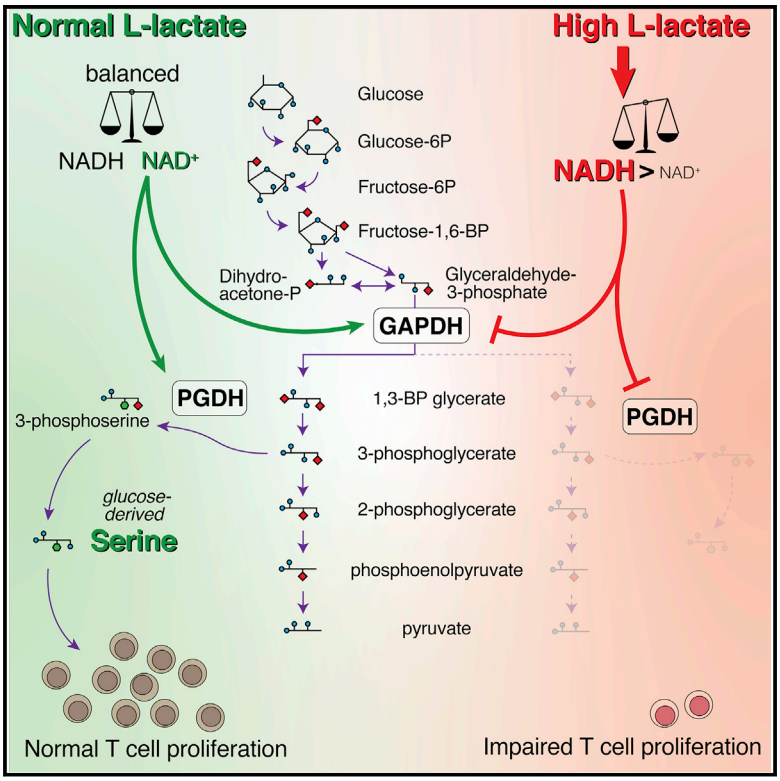

Highlights

- Lactate is metabolized by T cells and reduces NAD^+ to NADH
- NAD^+ reduction to NADH impairs glycolytic flux via GAPDH
- Lactate depletes post-GAPDH glycolytic intermediates and glucose-derived serine
- Adding serine rescues T cell proliferation from lactate-induced reductive stress

Authors

William J. Quinn III, Jing Jiao, Tara TeSlaa, ..., Douglas C. Wallace, Joseph A. Baur, Ulf H. Beier

Correspondence

beieru@email.chop.edu

In Brief

Quinn et al. report that lactate has an acidity-independent suppressive effect on effector T cell proliferation mediated through a shift from NAD^+ to NADH (lactate-induced reductive stress). This impairs glycolysis and glucose-derived serine production, which is required for effector T cell proliferation.

Quinn et al., 2020, Cell Reports *33*, 108500
December 15, 2020
https://doi.org/10.1016/j.celrep.2020.108500

Cell Reports

CellPress
OPEN ACCESS

Report

Lactate Limits T Cell Proliferation via the NAD(H) Redox State

William J. Quinn III,[1,12] Jing Jiao,[2,12] Tara TeSlaa,[3,12] Jason Stadanlick,[4] Zhonglin Wang,[5] Liqing Wang,[6] Tatiana Akimova,[6] Alessia Angelin,[7] Patrick M. Schäfer,[7] Michelle D. Cully,[2] Caroline Perry,[1] Piotr K. Kopinski,[7] Lili Guo,[8] Ian A. Blair,[8] Louis R. Ghanem,[9] Michael S. Leibowitz,[10] Wayne W. Hancock,[6] Edmund K. Moon,[11] Matthew H. Levine,[5] Evgeniy B. Eruslanov,[4] Douglas C. Wallace,[7] Joseph A. Baur,[1] and Ulf H. Beier[2,13,*]

[1]Department of Physiology and Institute of Diabetes, Obesity, and Metabolism, University of Pennsylvania, Philadelphia, PA 19104, USA
[2]Division of Nephrology and Department of Pediatrics, Children's Hospital of Philadelphia and University of Pennsylvania, Philadelphia, PA 19104, USA
[3]Lewis Sigler Institute for Integrative Genomics and Department of Chemistry, Princeton University, Washington Road, Princeton, NJ 08544, USA
[4]Division of Thoracic Surgery, Department of Surgery, Perelman School of Medicine at the University of Pennsylvania, Philadelphia, PA 19104, USA
[5]Department of Surgery, Penn Transplant Institute, Perelman School of Medicine, Children's Hospital of Philadelphia and University of Pennsylvania, Philadelphia, PA 19104, USA
[6]Division of Transplant Immunology, Department of Pathology and Laboratory Medicine and Biesecker Center for Pediatric Liver Disease, Children's Hospital of Philadelphia and University of Pennsylvania, Philadelphia, PA 19104, USA
[7]Center for Mitochondrial and Epigenomic Medicine, Children's Hospital of Philadelphia, Philadelphia, PA 19104, USA
[8]Penn SRP Center, Center of Excellence in Environmental Toxicology and Department of Systems Pharmacology and Translational Therapeutics, Perelman School of Medicine, University of Pennsylvania, Philadelphia, PA 19104, USA
[9]Division of Gastroenterology, Hepatology and Nutrition, Department of Pediatrics, Perelman School of Medicine at the University of Pennsylvania, Philadelphia, PA 19104, USA
[10]Division of Oncology, Department of Pediatrics, Perelman School of Medicine at the University of Pennsylvania, Philadelphia, PA 19104, USA
[11]Department of Medicine, Perelman School of Medicine at the University of Pennsylvania, Philadelphia, PA 19104, USA
[12]These authors contributed equally
[13]Lead Contact
*Correspondence: beieru@email.chop.edu
https://doi.org/10.1016/j.celrep.2020.108500

SUMMARY

Immune cell function is influenced by metabolic conditions. Low-glucose, high-lactate environments, such as the placenta, gastrointestinal tract, and the tumor microenvironment, are immunosuppressive, especially for glycolysis-dependent effector T cells. We report that nicotinamide adenine dinucleotide (NAD^+), which is reduced to NADH by lactate dehydrogenase in lactate-rich conditions, is a key point of metabolic control in T cells. Reduced NADH is not available for NAD^+-dependent enzymatic reactions involving glyceraldehyde 3-phosphate dehydrogenase (GAPDH) and 3-phosphoglycerate dehydrogenase (PGDH). We show that increased lactate leads to a block at GAPDH and PGDH, leading to the depletion of post-GAPDH glycolytic intermediates, as well as the 3-phosphoglycerate derivative serine that is known to be important for T cell proliferation. Supplementing serine rescues the ability of T cells to proliferate in the presence of lactate-induced reductive stress. Directly targeting the redox state may be a useful approach for developing novel immunotherapies in cancer and therapeutic immunosuppression.

INTRODUCTION

Immune-privileged tissues are able to restrict immune responses. Many of these sites, including the gastrointestinal tract, placenta, testis, and cornea but also ischemic tissues and the tumor microenvironment share overlapping metabolic characteristics, such as being glycolytic and enriched in lactic acid (Bax and Bloxam, 1997; Boussouar and Benahmed, 2004; Buck et al., 2017; Kinoshita, 1962). Understanding the mechanisms of these overlapping immunosuppressive metabolic conditions has promise for improving anti-tumor immunotherapy and may also aid in developing novel immunosuppressive therapies. Tumors have long been known to engage in aerobic glycolysis (Warburg et al., 1924). Glucose depletion and lactic acid production impair cytotoxic and effector T cells that require glycolysis to proliferate and produce cytokines (Chang et al., 2013, 2015; Ho et al., 2015; Menk et al., 2018). L-lactic acid lowers ambient pH, decreasing dendritic cell activation; impairs T cell glycolysis and effector T cell function; and is a key mediator of tumor-induced immunosuppression (Brand et al., 2016; Fischer et al., 2007; Marin et al.,

2019). Tumors with an impaired ability to produce L-lactic acid are contained in immunocompetent mice but grow well in mice lacking T and natural killer (NK) cells (Brand et al., 2016). Prior studies have highlighted the detrimental effects of acidity (Fischer et al., 2007), but there is also evidence of pH-independent effects; e.g., mice transplanted with fully mismatched cardiac allografts treated with either Na L-lactate or NaCl control injections show prolonged allograft survival (Angelin et al., 2017). These data, together with our prior observation of L-lactate inhibition of effector T cell proliferation being lactate dehydrogenase (LDH)-dependent (Angelin et al., 2017), led us to hypothesize that lactate-driven reduction of nicotinamide adenine dinucleotide (NAD^+) to NADH may deprive effector T cells of forward glycolytic flux at the NAD^+-dependent glyceraldehyde 3 phosphate dehydrogenase (GAPDH) reaction. We now demonstrate that the NAD redox state controls T cell glycolysis via GAPDH, as well as glucose-derived serine production. Our studies open new avenues to manipulate immune responses through NAD redox metabolism for the treatment of autoimmune diseases and immunosuppression, as well as for anti-tumor immunotherapy.

RESULTS AND DISCUSSION

L-Lactate Has pH-Independent Suppressive Effects on T Cell Proliferation

To discern the effects of pH-neutral lactate from lactic acid, we compared the suppressive effects of L-lactate versus NaCl and L-lactic acid against pH-matched HCl on the proliferation of co-stimulated murine $CD4^+CD25^-$ conventional T cells (Tconv) cultured in low-glucose media (30 mg × dL^{-1}). We added up to 20 mM L-lactate, which matches the lactate burden encountered by T cells in our murine (Figures S1A–S1C), and published human tumor data (Walenta et al., 1997, 2000). We observed that L-lactate and L-lactic acid had persistent suppressive, apoptosis-independent effects beyond their respective NaCl and HCl controls (Figures 1A and 1B). Dead cells were removed from flow cytometric analysis by gating only on live cells (Figure S1D). Notably, 20 mM L-lactic acid dropped our cell culture pH to 5.63 ± 0.04 (Figure S1C), well below *in vivo* tumor pH measurements (Estrella et al., 2013; Helmlinger et al., 1997; Martin and Jain, 1994), further arguing for an acidity-independent suppressive effect *in vivo*. Interestingly, the suppressive effects of L-lactate are less prominent if higher glucose concentrations are used (Angelin et al., 2017), suggestive of some effect through glycolysis. We and others have previously observed acidity-independent suppressive effects of L-lactate *in vivo* in the setting of transplantation and graft-versus-host disease models (Angelin et al., 2017; Marin et al., 2019). We also observed that injection of the biguanide phenformin into C57BL/6J mice caused a buffered increase in L-lactate (Figure 1C) and prolonged cardiac allograft survival (Figure 1D). In conclusion, L-lactate has pH-independent suppressive effects on T cell proliferation.

L-Lactate Interrupts Glycolytic Flux at the GAPDH Reaction

T cells are capable of taking up ambient lactate, and through [$^{13}C_3$] L-lactate tracing, we observed that L-lactate is metabolized to pyruvate and Krebs cycle intermediates (Figure 1E). We have previously observed that inhibiting the lactate dehydrogenase reaction, which reduces NAD^+ to NADH when lactate is oxidized, protects T cells from the suppressive effects of ambient L-lactate (Angelin et al., 2017). This led us to hypothesize that L-lactate may block the forward NAD^+-dependent GAPDH reaction (Figure 1F). Indeed, L-lactate reduced the NAD^+:NADH redox balance (Figure 1G). To assess whether the GAPDH reaction was affected by a shift in the NAD redox balance, we polarized NAD^+:NADH with L-lactate and pyruvate in stimulated murine Tconv and quantified glycolytic intermediates by liquid chromatography mass spectrometry (LC-MS). We found that adding 20 mM pH-neutral Na L-lactate led to an enrichment of pre- and a depletion of post-GAPDH glycolytic intermediates relative to NaCl control, similar to treatment with a GAPDH inhibitor (1 μM heptelidic acid; GAPDHi), although Na pyruvate had the opposite effect (Figure 1H). The apparent GAPDH block through L-lactate was supported by a reduction in glucose consumption by CD3ε/CD28 monoclonal antibody (mAb)-activated $CD8^+$ and $CD4^+$ T cells (Figures 1I and S1E). In conclusion, lactate reduces NAD^+ to NADH and blocks glycolysis by inhibiting GAPDH.

Lactate-Independent Alterations of the NAD^+:NADH Ratio Also Affect Glycolysis

Our observations that L-lactate may inhibit the forward GAPDH reaction through NAD^+ reduction to NADH led us to question whether other influences on the NAD^+:NADH ratio could produce similar effects. We took advantage of the principle that interruption of mitochondrial electron transport limits NADH oxidation, whereas uncoupling agents increase it (Duchen and Biscoe, 1992), and utilized oligomycin and rotenone to shift the NAD redox balance toward NADH and mitochondrial uncoupling to NAD^+ (Figures 2A–2D). Although the direct NAD^+:NADH redox effect is on the mitochondrial compartment, mitochondria are the major sink for cellular reducing equivalents and targeting this compartment also affects cytosolic NAD^+:NADH balance via malate-aspartate shuttling, as was demonstrated with mitochondrial overexpression of *Lactobacillus brevis* NADH oxidase (Titov et al., 2016). Next, we stimulated Tconv with CD3ε/CD28 mAb-coated beads and exposed them to oligomycin (reduced NADH), uncoupling through FCCP (oxidized NAD^+), and again impairment of NADH oxidation (rotenone and antimycin A). As expected, inhibition of mitochondrial ATP production increased extracellular acidification rates (ECARs) due to a compensatory increase in glycolysis (baseline to oligomycin; Figure 2E). We next observed that stimulated effector T cells exhibited a further increase in ECAR in the uncoupled state (oxidized NAD^+) above the oligomycin baseline (reduced NADH). The further increase in ECAR after adding FCCP on top of oligomycin cannot be explained by impairing mitochondrial ATP production, which had already been inhibited. Inhibiting electron transport chain complex I and/or III reduced NAD^+ to NADH and brought the ECAR back toward the oligomycin level (Figures 2E–2G). We interpret these data to mean that maximal glycolytic rate is higher under conditions where the NAD^+ pool is more oxidized and, conversely, that reductive stress can slow glycolytic flux. Of note, ECAR is often taken as a proxy for glycolytic flux; however,

CellPress
OPEN ACCESS

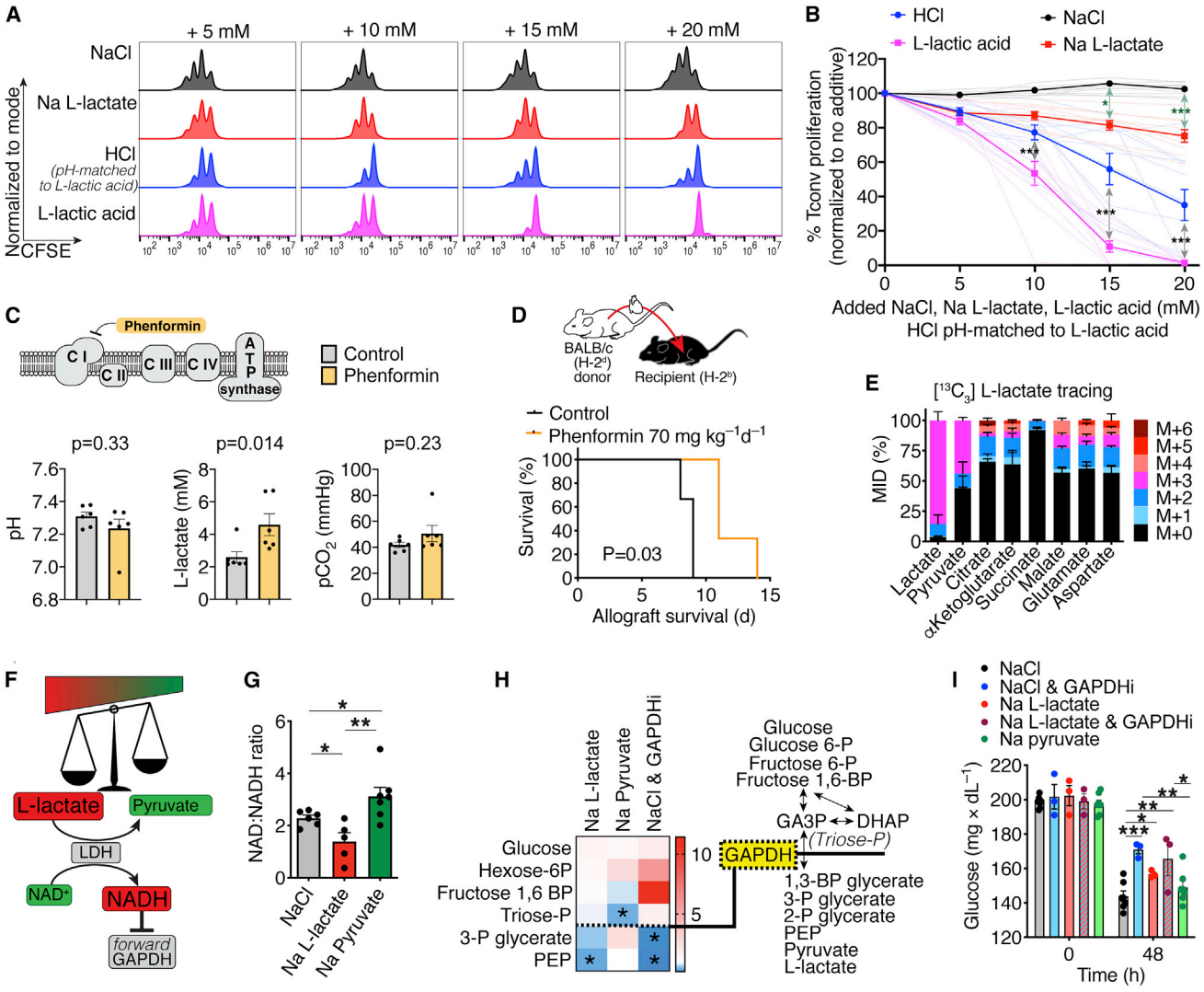

Figure 1. L-Lactate Lowers the NAD$^+$:NADH Ratio and Induces a GAPDH Block

(A and B) Murine CD4$^+$CD25$^-$ T cells were labeled with carboxyfluorescein succinimidyl ester (CFSE), co-stimulated for 3 days with anti-CD3ε/CD28-coated beads, and exposed to NaCl, Na L-lactate, HCl, and L-lactic acid at the indicated doses in low-glucose media (30 mg × dL^{-1}). The pH of the HCl condition was adjusted to match the L-lactic-acid-containing media. Teff proliferation was analyzed by CFSE dilution through flow cytometry. (A) shows representative and (B) pooled data from 11 independent experiments (two-way ANOVA with multiple comparison of treatment condition and dose).

(C and D) Phenformin (70 mg kg^{-1} day^{-1}) was administered to C57BL/6J mice.

(C) 2 h after phenformin injection, CG4$^+$ venous blood gas showed increased L-lactate (6/grp).

(D) C57BL/6J mice received an major histocompatibility complex (MHC)-mismatched BALB/c heart transplant and were treated with phenformin (70 mg kg^{-1} day^{-1}) for 14 days or DMSO vehicle control (3/grp, log rank [Mantel-Cox] test).

(E) L-lactate derivative analysis from modified media with 20 mM [$^{13}C_3$] L-lactate and 1.11 mM [$^{12}C_6$] D-glucose shows that 16 h anti-CD3ε/CD28 stimulated Tconvs oxidize L-lactate into pyruvate and metabolize it in the Krebs cycle. MID denotes mass isotopomer distribution, and M0–M6 denote the number of [^{13}C] per indicated molecule. Data are pooled from three independent experiments.

(F) Hypothesis: L-lactate-mediated reduction of NAD$^+$ to NADH blocks the GAPDH forward reaction.

(G) Tconvs were isolated from C57BL/6J mice and co-stimulated for 16 h with CD3ε/CD28 mAb-coated beads and 20 mM NaCl, Na lactate, or Na pyruvate. NAD:NADH was measured by cycling. Pyruvate increased although lactate decreased the proportion of oxidized NAD$^+$. Data are pooled from seven independent experiments (paired one-way ANOVA).

(H) Tconvs were stimulated with CD3ε/CD28 mAb-coated beads and cultured in low-glucose medium (30 mg × dL^{-1}) for 48 h ± 20 mM NaCl, Na L-lactate, or Na pyruvate and 1 μM heptelidic acid (GAPDHi) or vehicle control (H_2O). Metabolites were extracted and analyzed via LC-MS. The heatmap shows increased (red) and decreased (blue) glycolytic intermediates ion count normalized to the NaCl and vehicle control (dotted line indicates GAPDH reaction). Addition of Na pyruvate led to a depletion of pre-GAPDH triose phosphate, although Na L-lactate (NADH reduction) led to a decline in post-GAPDH metabolites, similar to direct GAPDH inhibition.

(I) 10^6 CD8$^+$ T cells were co-stimulated and cultured with ±20 mM NaCl, Na L-lactate, GAPDHi, or Na pyruvate, and glucose was measured in the supernatant. Data are pooled from seven independent experiments (one-way ANOVA). *p < 0.05, **p < 0.01, and ***p < 0.001. Error bars indicate SEM.

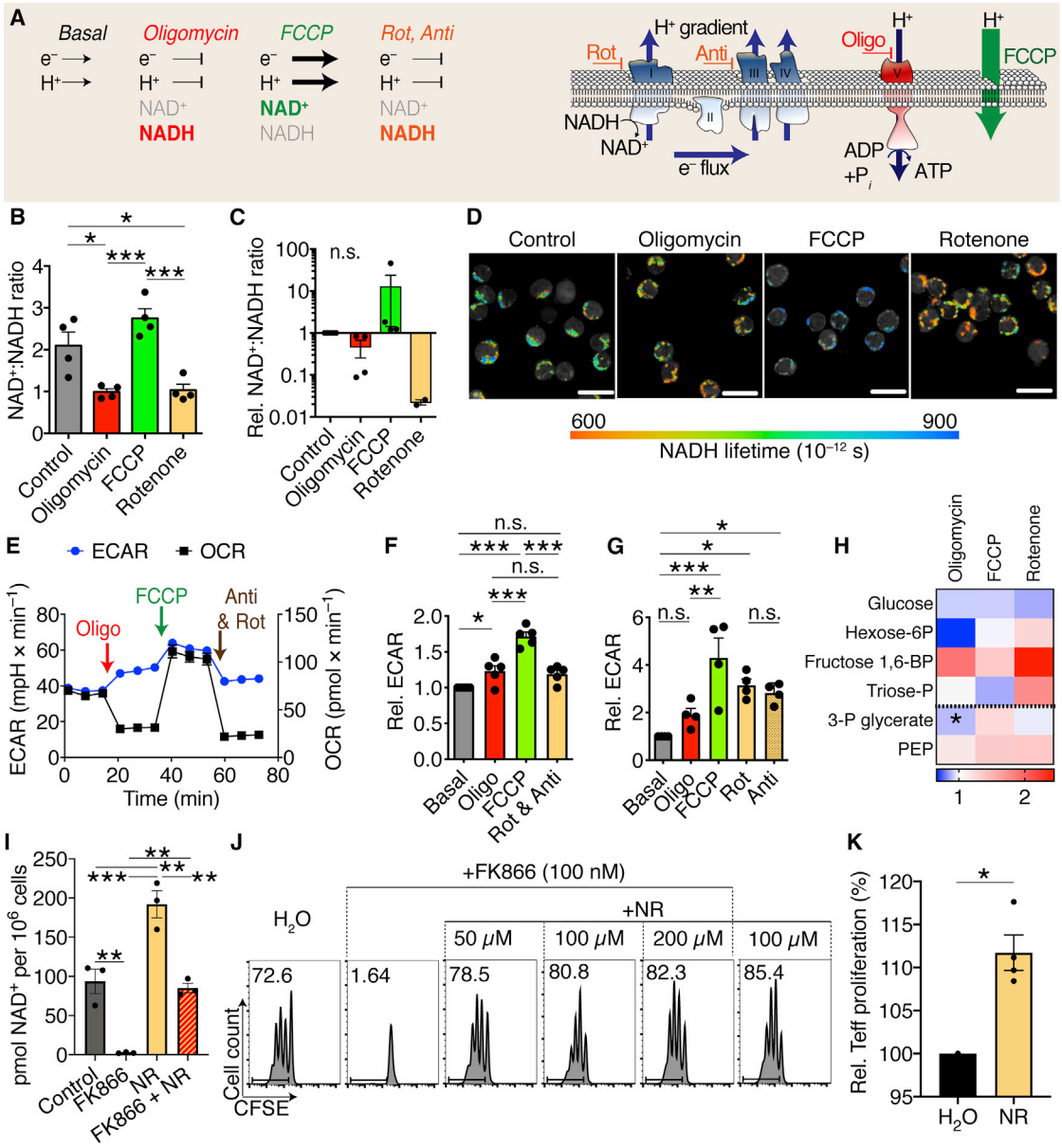

Figure 2. Reduced NAD$^+$:NADH Redox State Limits Glycolysis in T Cells

(A) Schematic of the electron transport chain (ETC) complexes I–V at the inner mitochondrial membrane with complex V denoting ATP synthase and how oligomycin (oligo), FCCP (cyanide-4-[trifluoromethoxy]phenylhydrazone), rotenone (Rot), and antimycin (anti) can act as NAD:NADH polarizing agents.

(B and C) Tconvs were stimulated with CD3ε/CD28 mAb-coated beads for 48 h and then exposed to 1.25 μM oligomycin, 1 μM FCCP, or 1 μM rotenone for 15 min. NAD and NADH were measured by (B) NAD cycling or (C) LC-MS (paired one-way ANOVA; four independent experiments). Oligomycin and rotenone increased NADH reduction, although mitochondrial uncoupling (FCCP) increased NAD oxidation.

(D) Tconvs were stimulated with CD3ε/CD28 soluble mAb and exposed to oligomycin, FCCP, or rotenone as in (B) and (C). Fluorescence lifetime imaging microscopy showed prolonged NADH autofluorescence with FCCP uncoupling, consistent with mitochondrial NAD oxidation. Scale bar, 10 μm. Data are representative of four independent experiments.

(E–G) Tconv cells were stimulated with anti-CD3ε/CD28 beads and 25 U interleukin-2 (IL-2) × mL^{-1} for 16 h (E and F) or 2 h (G). Oligomycin increases ECAR as expected. In stimulated Tconv, mitochondrial uncoupling (oxidized NAD$^+$) through FCCP further increases ECAR, which can be brought back to the oligomycin level via rotenone and antimycin (reduced NADH). (E) shows representative and (F) and (G) pooled data from five (F) and four (G) independent experiments, respectively (paired one-way ANOVA).

(H) LC-MS total ion counts of glycolysis metabolites from Tconv treated as in (C). *$p < 0.05$ (Student's t test versus untreated; data pooled from four independent experiments). Dotted line indicates GAPDH reaction.

(legend continued on next page)

Krebs cycle activity can also contribute measurably to acidification via CO_2 production (Mookerjee et al., 2015). To ensure that the observations made in T cell ECAR translate to other modalities of assessing glycolytic activity, we confirmed the effects of oligomycin, FCCP, and rotenone on pre- and post-glycolytic intermediates via LC-MS, where we observe that the NADH reduced states (oligomycin and rotenone) tended to have higher pre- and lower post-GAPDH glycolytic intermediates than in the uncoupled NAD^+ oxidized state (Figure 2H). Interestingly, the NAD^+:NADH dependence of glycolytic flux was limited to glycolytic effector T cells. In freshly isolated, unstimulated $CD4^+CD25^-$ T cells, which are not glycolytic (van der Windt and Pearce, 2012), no significant difference between oligomycin and FCCP was seen (Figure S2A). Likewise, we did not observe an increase in ECAR when adding FCCP to oligomycin-exposed regulatory T cells (T reg cells), which are also non-glycolytic (Angelin et al., 2017; Gerriets et al., 2016; Howie et al., 2017), or in non-glycolytic renal tubular epithelial cells (Figures S2B–S2E). In contrast, we observed a pattern of increased ECAR with uncoupling relative to oligomycin in other glycolytic non-T cells, such as murine myo- and fibroblasts (Figures S2F–S2H). We conclude from these data that changing NAD^+:NADH ratios by manipulating the electron transport chain results in altered ECAR in glycolytic effector T cells.

Augmenting NAD^+ Recycling through Nicotinamide Riboside Increases T Cell Proliferation

The observation that lactate can impair T cell proliferation through a redox shift from NAD^+ to NADH led us to question whether the increase in NADH or simply the reduced availability of NAD^+ was key to the effect. To deplete NAD^+ without increasing NADH, we used FK866, an inhibitor of NAD recycling. Nicotinamide riboside was used as a rescue condition to restore NAD^+ independent of the enzyme inhibited by FK866 (Frederick et al., 2016). We observed that depleting total NAD^+ via FK866 was toxic (Figures 2I and 2J). Interestingly, nicotinamide riboside supplementation alone was sufficient to increase Teff proliferation in low-glucose media (Figures 2J and 2K). These data suggested that the availability of oxidized NAD^+ is the relevant parameter for T cell proliferation, and methods to increase the pool of available NAD^+ may be of use to boost the ability of T cell to proliferate.

L-Lactate Depletes Post-GAPDH Glycolytic Intermediates and Serine

To assess GAPDH reaction kinetics, we utilized [$^{13}C_6$] D-glucose and [$^{13}C_3$] pyruvate tracing. Similar to Marin et al. (2019), we noted an overall decline in T cell glycolysis; however, this was restricted to post-GAPDH glycolytic intermediates, including phosphoenolpyruvate (PEP) and pyruvate, although the reverse GAPDH reaction was unaffected (Figure S3). A depletion of PEP could impair T cell proliferation through a reduction of intracellular calcium (Ho et al., 2015; Vaeth et al., 2017). We tested this hypothesis by restoring intracellular calcium through ionomycin, which rescued the L-lactate phenotype (Figures 3A and 3B). We observed a similar phenotype for D-lactate and with calcium re-uptake inhibition (Figures S4A–S4C). In addition, through flow-cytometric calcium measurements, we noted that Na lactate reduced intracellular calcium (Figures S4D–S4F). To validate that PEP rather than calcium was required to rescue L-lactate-inhibited T cell proliferation, we added oxalate, which inhibits pyruvate kinase and stabilizes PEP (Ho et al., 2015). We observed that adding oxalate only marginally improved L-lactate-meditated T cell suppression (Figures 3C–3E). In addition, downstream of calcium, the phosphorylation state of the nuclear factor of activated T cells (NFAT) was unaffected by NAD redox polarization, and pharmacologic calcium manipulations did not alter the NAD redox state beyond toxicity (Figures S4G–S4I). These data led us to assess calcium-independent effects mediating lactate-induced T cell suppression and, in particular, glucose-derived serine production, which was shown to be important for T cell proliferation (Ma et al., 2017). Indeed, a key enzyme in this pathway, phosphoglycerate dehydrogenase (PGDH) is also NAD^+ dependent and thus vulnerable to lactate-induced reductive stress. We observed that, in contrast to oxalate, serine could fully rescue lactate-mediated T cell suppression (Figures 3C–3E). To validate the observations in the rescue experiments, we repeated the [$^{13}C_6$] D-glucose tracing experiment in serine and glycine free media. We observed that pre-GAPDH glycolytic intermediates were enriched with both the addition of L-lactate and oxalate (Figures 4A–4E). Post-GAPDH, we noted that oxalate increased glucose-derived PEP as expected (Figures 4F–4J). Glucose-derived serine was diminished with L-lactate (Figures 4K–4M). These data supported serine deficiency due to L-lactate-induced reductive stress in proliferating T cells. In fact, oxalate also partially increased glucose-derived serine production through the pyruvate kinase block, which could contribute to the partial rescue effect with oxalate (Figures 3D and 3E). In contrast, the pentose phosphate pathway, which branches off prior to the GAPDH reaction, showed an increased abundance of isotopologues with glucose-derived carbons with both lactate and oxalate (Figure 4N). Glucose-derived serine and subsequently glycine is a key contributor to purine synthesis. We found that both ATP and ADP appeared with an equal M+5 labeling, potentially derived from ribose-5-phosphate, but had less M+7 to M+9 labeling, which could indicate impaired glucose-derived purine synthesis (Figures 4O and S3L). Taken together, our data show that L-lactate limits glucose-derived serine production, which is important to T cell proliferation.

(I) NAD and NADH measurements in murine Tconv-stimulated CD3ε/CD28 mAb-coated beads for 3 days and exposed to the nicotinamide phosphoribosyltransferase (Nampt) inhibitor FK866 at 100 nM with or without 100 μM of the NAD precursor nicotinamide riboside (NR). Data are pooled from three independent experiments (one-way ANOVA).

(J) Murine Tconvs were CFSE labeled and stimulated with CD3ε/CD28 mAb for 3 days in low-glucose media (30 mg × dL^{-1}). Adding 100 nM FK866 to inhibit NAD regeneration was toxic to dividing T cells. Enriching NAD^+ through administration of NR rescued the dividing T cells from FK866 toxicity. Adding NR along augmented T cell proliferation is shown.

(K) Quantitative data to added NR in low-glucose media; data pooled from four independent experiments (paired Student's t test).

*$p < 0.05$, **$p < 0.01$, and ***$p < 0.001$. Error bars indicate SEM.

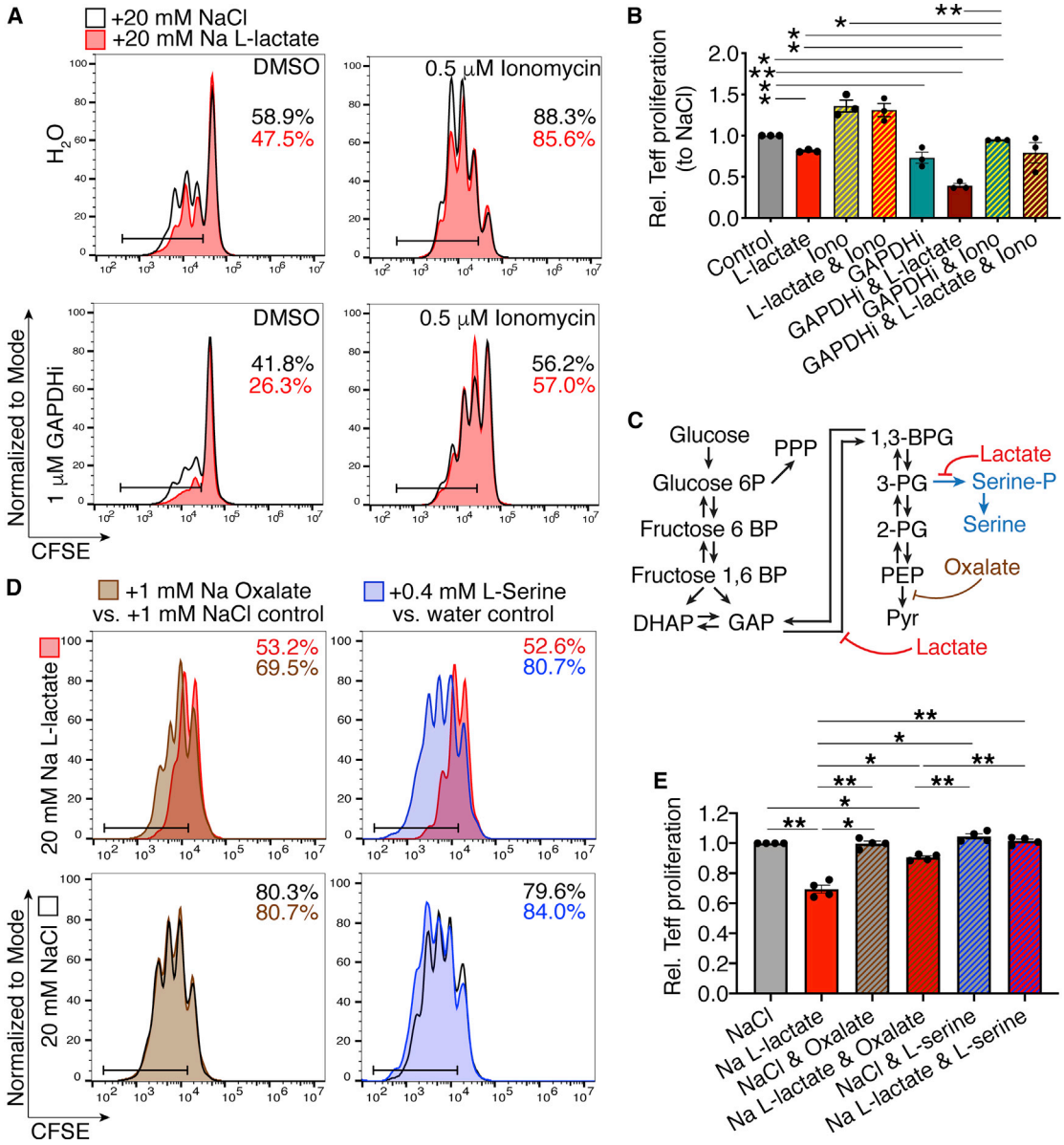

Figure 3. L-Lactate Depletes Post-GAPDH Glycolytic Intermediates

(A and B) Tconvs were co-stimulated with CD3ε/CD28 mAb-coated beads and cultured in low-glucose medium (30 mg × dL^{-1}) ± 20 mM NaCl or Na L-lactate, with either 0.5 μM ionomycin, 1 μM of the GAPDH inhibitor (GAPDHi) heptelidic acid, or vehicle controls. After 3 days, proliferation was analyzed via CFSE dilution. (A) shows representative and (B) quantitative data pooled from three independent experiments (paired one-way ANOVA).

(C) Lactate inhibits GAPDH and PGDH, although oxalate blocks pyruvate kinase.

(D and E) Tconvs were co-stimulated with CD3ε/CD28 mAb-coated beads and cultured in low-glucose medium (30 mg × dL^{-1}) in serine/glycine-free media ± 20 mM NaCl or Na L-lactate, with either 0.4 mM serine or 1 mM Na oxalate or vehicle controls. After 3 days, proliferation was analyzed via CFSE dilution. (D) shows representative and (E) quantitative data pooled from four independent experiments (paired one-way ANOVA).

*$p < 0.05$, **$p < 0.01$, and ***$p < 0.001$. Error bars indicate SEM.

The Role of the NAD^+:NADH Redox State in T Cell Function

Our observation that NAD-redox metabolism is important for T cell glycolysis and proliferation could point toward a generalizable mechanism of peripheral tolerance. A low intracellular NAD^+:NADH ratio generated by high levels of ambient lactate, which is common in immune-privileged tissues and in the tumor microenvironment, could reshape T cells toward a suppressed, pro-tolerant state. Once T cells migrate out of these immune-privileged environments, less lactate is taken up by the T cells, allowing the NAD^+:NADH ratio to recover, restoring the ability to produce serine from glucose and thereby re-enabling physiologic immunity. Although there are exceptions to this principle, such as proinflammatory effects of lactate in chronic

CellPress
OPEN ACCESS

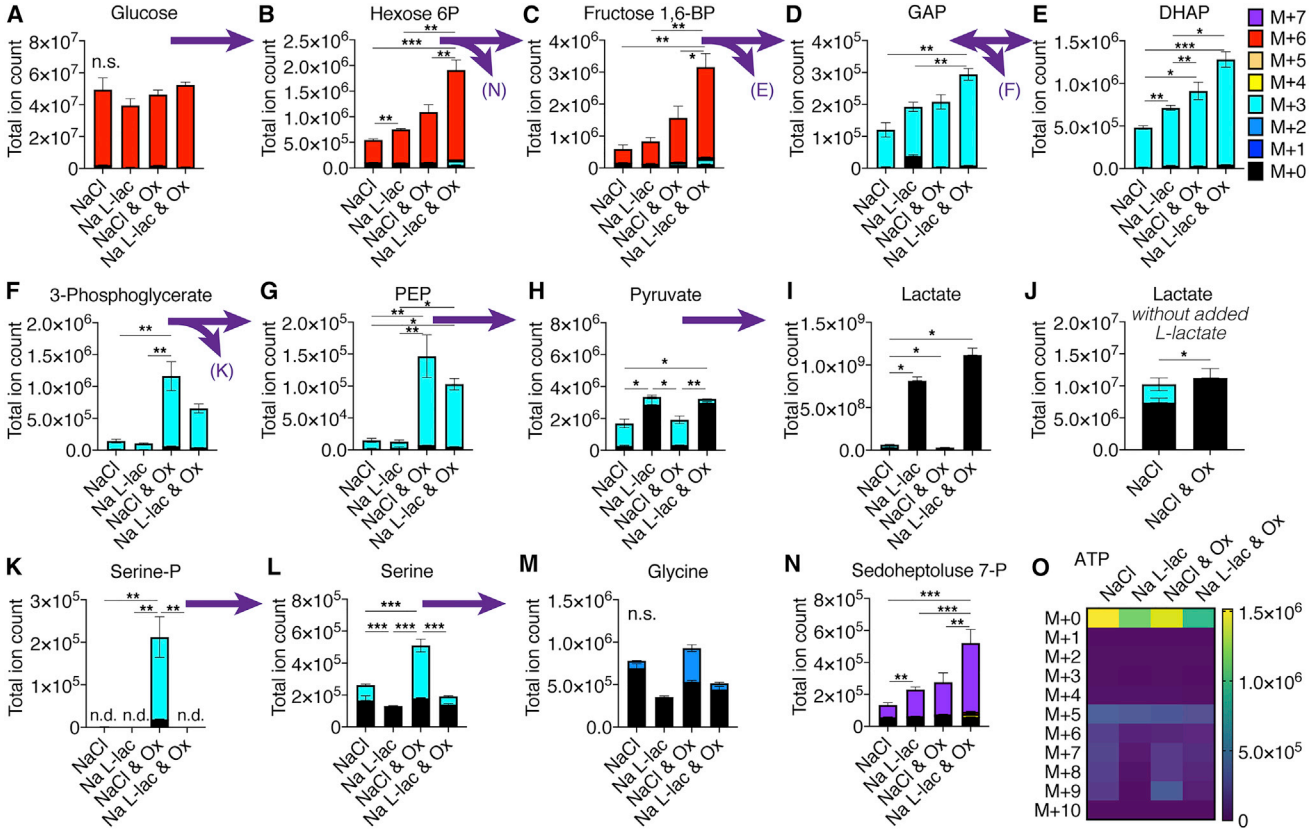

Figure 4. L-Lactate Impairs Glucose-Derived Serine Production

Tconvs were co-stimulated with CD3ε/CD28 mAb-coated beads for 20 h and were then labeled with [$^{13}C_6$] D-glucose in serine and glycine free media for 3 h with either 20 mM of NaCl or Na L-lactate (L-lac) and 1 mM NaCl or Na oxalate (Ox). Metabolites were extracted and analyzed for derivative analysis, with M+1–10 indicating the number of [^{13}C] labeling per molecule.

(A–E) Prior to GAPDH, L-lactate and oxalate lead to an accumulation of M+6 glucose and M+3 triose-P. Oxalate and lactate also lead to some reverse glycolysis (M+3 tracing in hexose 6P and fructose 1,6-BP).

(F–J) Post-GAPDH glycolytic intermediates: oxalate inhibits pyruvate kinase reaction. Both L-lactate and oxalate diminish the amount of pyruvate made from glucose.

(K–M) L-lactate decreases and oxalate increases glucose-derived serine.

(N) The pentose phosphate pathway is not diminished by L-lactate, if anything augmented by L-lactate/oxalate.

(O) Heatmap of total ion counts of ATP shows equal M+5 but diminished M+7 to M+9 with L-lactate treatment. Data are derived from three independent samples per condition (one-way ANOVA or Student's t test of the highest enriched isotopologue).

inflammation (Pucino et al., 2019), the fact that lactate is enriched in essentially all sites of immune privilege is probably of physiologic significance. This is despite different causes for lactic acid accumulation, such as preferred pyruvate to lactate reduction in the placenta (Markovic et al., 2018) or exogenous lactate production by commensal bacteria (Ménard et al., 2004). It may also be an additional physiologic explanation for glycolytic brain metabolism (Hui et al., 2017) and perhaps protect organisms from developing autoimmune responses during an ischemic or traumatic injury. There are several potential therapeutic applications of our data. Increasing the NAD^+:NADH ratio may aid in strengthening immune responses against cancer or even infection. This could be achieved through NAD-oxidizing agents, some of which are already proposed as anti-cancer treatments (Li et al., 1999; Ough et al., 2005); supplementation of NAD^+ precursors, such as nicotinamide riboside (Liu et al., 2018); augmenting NADH oxidation by expressing NADH oxidase (Titov et al., 2016); or by augmenting mitochondrial function and oxidative phosphorylation of T cells (Kawalekar et al., 2016; Scharping et al., 2016). Altering NAD^+ transport between the cytoplasm and mitochondria (Luongo et al., 2020) may modify the ability of T cells to buffer redox stress. In addition, efforts to limit L-lactic acid efflux from tumors can augment anti-tumor immune responses (Renner et al., 2019).

Given our observation of lactate impairing T cell proliferation through glucose-derived serine production and the established importance of glucose-derived serine for T cell proliferation (Ma et al., 2017), it is important to consider unintended adverse consequences to serine/glycine-depleted diets aimed at impairing tumor growth (Amelio et al., 2017), as these could harm, in particular, intra-tumoral T cells, which are already under lactate-induced reductive stress. It is possible that, under

some circumstances, serine may even augment anti-tumor immune responses.

Aside from anti-tumor immunotherapy, there are therapeutic opportunities for immunosuppressive applications based upon a decreased NAD^+:NADH redox balance, such as utilizing L-lactic-acid-producing bacteria to utilize the immunosuppressive effects of lactate (Ghouri et al., 2014), or by adoptively transferring L-lactic-acid-producing dendritic cells to treat graft-versus-host disease (Marin et al., 2019). In light of substantial toxicity from conventional immunosuppressive drugs (Fishman, 2007; Naesens et al., 2009; Shivaswamy et al., 2016), it is conceivable to consider lactate supplementation and dietary serine restriction to perhaps allow lower dosing in conventional immunosuppressive therapies.

In conclusion, we have shown that lactate can impair T cell proliferation independent from microenvironment acidification by reductive stress, which depletes the GAPDH and PGDH reactions of NAD^+ and deprives proliferating T cells of glucose-derived serine. These findings indicate a joint mechanism of immune-privileged tissues and the tumor microenvironment, which share high-lactate environments. Manipulation of NAD redox metabolism or lactate levels may open novel approaches to selectively promote immune modulation to augment anti-tumor immunity or achieve therapeutic immunosuppression.

STAR★METHODS

Detailed methods are provided in the online version of this paper and include the following:

- KEY RESOURCES TABLE
- RESOURCE AVAILABILITY
  - Lead contact
  - Materials availability
  - Data and code availability
- EXPERIMENTAL MODEL AND SUBJECT DETAILS
  - Mice
  - Cell lines
  - Cell culture media and cell culture conditions
- METHOD DETAILS
  - Bioenergetic measurements
  - Blood gas measurements
  - Cardiac allografting
  - Cell isolation and flow cytometry
  - Fluorescence Lifetime Imaging Microscopy (FLIM)
  - Glucose and L-lactate measurements
  - Heavy carbon tracer labeling
  - Immunoblotting
  - Metabolite extraction and derivatization
  - NAD^+:NADH cycling assay
  - Liquid chromatography mass spectrometry and reaction monitoring
  - Tumor lactate measurements
- QUANTIFICATION AND STATISTICAL ANALYSIS

SUPPLEMENTAL INFORMATION

Supplemental Information can be found online at https://doi.org/10.1016/j.celrep.2020.108500.

ACKNOWLEDGMENTS

We thank Benjamin Philipson, Roddy S. O'Connor, Michael C. Milone, and Steven M. Albelda (all U. Penn) for helpful comments. We thank Joshua D. Rabinowitz and the Penn IDOM metabolomics core for advice on the tracing and mass spectroscopy studies. Financial support was as follows: NIH grant AI095353, Laffey-McHugh Foundation, and American Society of Nephrology funding (to U.H.B.); 1F32DK118856 (to T.T.); NIH grants DK098656 and AG043483 (to J.A.B.), DK106243 (to M.H.L.), and AI073489 and AI095276 (to W.W.H.); HHMI International Student Research fellowship (to P.K.K.); and NIH grants NS021328, MH108592, and OD010944 and Department of Defense grant W81XWH-16-1-0401 (to D.C.W.).

AUTHOR CONTRIBUTIONS

Conceptualization, U.H.B., W.J.Q., and J.A.B.; Methodology, T.T., P.M.S., and E.B.E.; Investigation, J.J., W.J.Q., T.T., U.H.B., J.S., Z.W., C.P., L.W., L.R.G., M.S.L., T.A., A.A., M.D.C., P.M.S., and P.K.K.; Analysis, U.H.B., J.A.B., W.J.Q., T.A., W.W.H., M.H.L., I.A.B., P.M.S., and D.C.W.; Resources, D.C.W. and E.K.M.; Writing—Original Draft, U.H.B.; Writing—Review and Editing, J.A.B., T.T., W.J.Q., and W.W.H.

DECLARATION OF INTERESTS

The authors declare no competing interests.

Received: January 17, 2020
Revised: October 8, 2020
Accepted: November 18, 2020
Published: December 15, 2020

SUPPORTING CITATIONS

The following references appear in the Supplemental Information: Ewaschuk et al., 2005; Flick and Konieczny, 2002.

REFERENCES

Amelio, I., Melino, G., and Frezza, C. (2017). Exploiting tumour addiction with a serine and glycine-free diet. Cell Death Differ. *24*, 1311–1313.

Angelin, A., Gil-de-Gómez, L., Dahiya, S., Jiao, J., Guo, L., Levine, M.H., Wang, Z., Quinn, W.J., 3rd, Kopinski, P.K., Wang, L., et al. (2017). Foxp3 reprograms T cell metabolism to function in low-glucose, high-lactate environments. Cell Metab. *25*, 1282–1293.e7.

Bax, B.E., and Bloxam, D.L. (1997). Energy metabolism and glycolysis in human placental trophoblast cells during differentiation. Biochim. Biophys. Acta *1319*, 283–292.

Beier, U.H., Angelin, A., Akimova, T., Wang, L., Liu, Y., Xiao, H., Koike, M.A., Hancock, S.A., Bhatti, T.R., Han, R., et al. (2015). Essential role of mitochondrial energy metabolism in Foxp3$^+$ T-regulatory cell function and allograft survival. FASEB J. *29*, 2315–2326.

Boussouar, F., and Benahmed, M. (2004). Lactate and energy metabolism in male germ cells. Trends Endocrinol. Metab. *15*, 345–350.

Brand, A., Singer, K., Koehl, G.E., Kolitzus, M., Schoenhammer, G., Thiel, A., Matos, C., Bruss, C., Klobuch, S., Peter, K., et al. (2016). LDHA-associated lactic acid production blunts tumor immunosurveillance by T and NK cells. Cell Metab. *24*, 657–671.

Buck, M.D., Sowell, R.T., Kaech, S.M., and Pearce, E.L. (2017). Metabolic instruction of immunity. Cell *169*, 570–586.

Chang, C.H., Curtis, J.D., Maggi, L.B., Jr., Faubert, B., Villarino, A.V., O'Sullivan, D., Huang, S.C., van der Windt, G.J., Blagih, J., Qiu, J., et al. (2013). Posttranscriptional control of T cell effector function by aerobic glycolysis. Cell *153*, 1239–1251.

Chang, C.H., Qiu, J., O'Sullivan, D., Buck, M.D., Noguchi, T., Curtis, J.D., Chen, Q., Gindin, M., Gubin, M.M., van der Windt, G.J., et al. (2015). Metabolic

competition in the tumor microenvironment is a driver of cancer progression. Cell *162*, 1229–1241.

Duchen, M.R., and Biscoe, T.J. (1992). Mitochondrial function in type I cells isolated from rabbit arterial chemoreceptors. J. Physiol. *450*, 13–31.

Estrella, V., Chen, T., Lloyd, M., Wojtkowiak, J., Cornnell, H.H., Ibrahim-Hashim, A., Bailey, K., Balagurunathan, Y., Rothberg, J.M., Sloane, B.F., et al. (2013). Acidity generated by the tumor microenvironment drives local invasion. Cancer Res. *73*, 1524–1535.

Ewaschuk, J.B., Naylor, J.M., and Zello, G.A. (2005). D-lactate in human and ruminant metabolism. J. Nutr. *135*, 1619–1625.

Fischer, K., Hoffmann, P., Voelkl, S., Meidenbauer, N., Ammer, J., Edinger, M., Gottfried, E., Schwarz, S., Rothe, G., Hoves, S., et al. (2007). Inhibitory effect of tumor cell-derived lactic acid on human T cells. Blood *109*, 3812–3819.

Fishman, J.A. (2007). Infection in solid-organ transplant recipients. N. Engl. J. Med. *357*, 2601–2614.

Flick, M.J., and Konieczny, S.F. (2002). Identification of putative mammalian D-lactate dehydrogenase enzymes. Biochem. Biophys. Res. Commun. *295*, 910–916.

Frederick, D.W., Loro, E., Liu, L., Davila, A., Jr., Chellappa, K., Silverman, I.M., Quinn, W.J., 3rd, Gosai, S.J., Tichy, E.D., Davis, J.G., et al. (2016). Loss of NAD homeostasis leads to progressive and reversible degeneration of skeletal muscle. Cell Metab. *24*, 269–282.

Gerriets, V.A., Kishton, R.J., Johnson, M.O., Cohen, S., Siska, P.J., Nichols, A.G., Warmoes, M.O., de Cubas, A.A., MacIver, N.J., Locasale, J.W., et al. (2016). Foxp3 and Toll-like receptor signaling balance T_{reg} cell anabolic metabolism for suppression. Nat. Immunol. *17*, 1459–1466.

Ghouri, Y.A., Richards, D.M., Rahimi, E.F., Krill, J.T., Jelinek, K.A., and DuPont, A.W. (2014). Systematic review of randomized controlled trials of probiotics, prebiotics, and synbiotics in inflammatory bowel disease. Clin. Exp. Gastroenterol. *7*, 473–487.

Graeff, R., and Lee, H.C. (2002). A novel cycling assay for cellular cADP-ribose with nanomolar sensitivity. Biochem. J. *361*, 379–384.

Helmlinger, G., Yuan, F., Dellian, M., and Jain, R.K. (1997). Interstitial pH and pO2 gradients in solid tumors in vivo: high-resolution measurements reveal a lack of correlation. Nat. Med. *3*, 177–182.

Ho, P.C., Bihuniak, J.D., Macintyre, A.N., Staron, M., Liu, X., Amezquita, R., Tsui, Y.C., Cui, G., Micevic, G., Perales, J.C., et al. (2015). Phosphoenolpyruvate is a metabolic checkpoint of anti-tumor T cell responses. Cell *162*, 1217–1228.

Howie, D., Cobbold, S.P., Adams, E., Ten Bokum, A., Necula, A.S., Zhang, W., Huang, H., Roberts, D.J., Thomas, B., Hester, S.S., et al. (2017). Foxp3 drives oxidative phosphorylation and protection from lipotoxicity. JCI Insight *2*, e89160.

Hui, S., Ghergurovich, J.M., Morscher, R.J., Jang, C., Teng, X., Lu, W., Esparza, L.A., Reya, T., Le Zhan, Yanxiang Guo, J., et al. (2017). Glucose feeds the TCA cycle via circulating lactate. Nature *551*, 115–118.

Jackaman, C., Bundell, C.S., Kinnear, B.F., Smith, A.M., Filion, P., van Hagen, D., Robinson, B.W., and Nelson, D.J. (2003). IL-2 intratumoral immunotherapy enhances CD8+ T cells that mediate destruction of tumor cells and tumor-associated vasculature: a novel mechanism for IL-2. J. Immunol. *171*, 5051–5063.

Kawalekar, O.U., O'Connor, R.S., Fraietta, J.A., Guo, L., McGettigan, S.E., Posey, A.D., Jr., Patel, P.R., Guedan, S., Scholler, J., Keith, B., et al. (2016). Distinct signaling of coreceptors regulates specific metabolism pathways and impacts memory development in CAR T cells. Immunity *44*, 380–390.

Kinoshita, J.H. (1962). Some aspects of the carbohydrate metabolism of the cornea. Invest. Ophthalmol. *1*, 178–186.

Levine, M.H., Wang, Z., Xiao, H., Jiao, J., Wang, L., Bhatti, T.R., Hancock, W.W., and Beier, U.H. (2016). Targeting Sirtuin-1 prolongs murine renal allograft survival and function. Kidney Int. *89*, 1016–1026.

Li, C.J., Li, Y.Z., Pinto, A.V., and Pardee, A.B. (1999). Potent inhibition of tumor survival in vivo by beta-lapachone plus taxol: combining drugs imposes different artificial checkpoints. Proc. Natl. Acad. Sci. USA *96*, 13369–13374.

Liu, L., Su, X., Quinn, W.J., 3rd, Hui, S., Krukenberg, K., Frederick, D.W., Redpath, P., Zhan, L., Chellappa, K., White, E., et al. (2018). Quantitative analysis of NAD synthesis-breakdown fluxes. Cell Metab. *27*, 1067–1080.e5.

Luongo, T.S., Eller, J.M., Lu, M.-J., Niere, M., Raith, F., Perry, C., Bornstein, M.R., Oliphint, P., Wang, L., McReynolds, M.R., et al. (2020). SLC25A51 is a mammalian mitochondrial NAD^+ transporter. Nature, Published online September 9, 2020. https://doi.org/10.1038/s41586-020-2741-7.

Ma, E.H., Bantug, G., Griss, T., Condotta, S., Johnson, R.M., Samborska, B., Mainolfi, N., Suri, V., Guak, H., Balmer, M.L., et al. (2017). Serine is an essential metabolite for effector T cell expansion. Cell Metab. *25*, 345–357.

Marin, E., Bouchet-Delbos, L., Renoult, O., Louvet, C., Nerriere-Daguin, V., Managh, A.J., Even, A., Giraud, M., Vu Manh, T.P., Aguesse, A., et al. (2019). Human tolerogenic dendritic cells regulate immune responses through lactate synthesis. Cell Metab. *30*, 1075–1090.e8.

Markovic, S., Fages, A., Roussel, T., Hadas, R., Brandis, A., Neeman, M., and Frydman, L. (2018). Placental physiology monitored by hyperpolarized dynamic ^{13}C magnetic resonance. Proc. Natl. Acad. Sci. USA *115*, E2429–E2436.

Martin, G.R., and Jain, R.K. (1994). Noninvasive measurement of interstitial pH profiles in normal and neoplastic tissue using fluorescence ratio imaging microscopy. Cancer Res. *54*, 5670–5674.

Melamud, E., Vastag, L., and Rabinowitz, J.D. (2010). Metabolomic analysis and visualization engine for LC-MS data. Anal. Chem. *82*, 9818–9826.

Ménard, S., Candalh, C., Bambou, J.C., Terpend, K., Cerf-Bensussan, N., and Heyman, M. (2004). Lactic acid bacteria secrete metabolites retaining anti-inflammatory properties after intestinal transport. Gut *53*, 821–828.

Menk, A.V., Scharping, N.E., Moreci, R.S., Zeng, X., Guy, C., Salvatore, S., Bae, H., Xie, J., Young, H.A., Wendell, S.G., and Delgoffe, G.M. (2018). Early TCR signaling induces rapid aerobic glycolysis enabling distinct acute T cell effector functions. Cell Rep. *22*, 1509–1521.

Mookerjee, S.A., Goncalves, R.L.S., Gerencser, A.A., Nicholls, D.G., and Brand, M.D. (2015). The contributions of respiration and glycolysis to extracellular acid production. Biochim. Biophys. Acta *1847*, 171–181.

Naesens, M., Kuypers, D.R., and Sarwal, M. (2009). Calcineurin inhibitor nephrotoxicity. Clin. J. Am. Soc. Nephrol. *4*, 481–508.

Ough, M., Lewis, A., Bey, E.A., Gao, J., Ritchie, J.M., Bornmann, W., Boothman, D.A., Oberley, L.W., and Cullen, J.J. (2005). Efficacy of beta-lapachone in pancreatic cancer treatment: exploiting the novel, therapeutic target NQO1. Cancer Biol. Ther. *4*, 95–102.

Pucino, V., Certo, M., Bulusu, V., Cucchi, D., Goldmann, K., Pontarini, E., Haas, R., Smith, J., Headland, S.E., Blighe, K., et al. (2019). Lactate buildup at the site of chronic inflammation promotes disease by inducing $CD4^+$ T cell metabolic rewiring. Cell Metab. *30*, 1055–1074.e8.

Renner, K., Bruss, C., Schnell, A., Koehl, G., Becker, H.M., Fante, M., Menevse, A.-N., Kauer, N., Blazquez, R., Hacker, L., et al. (2019). Restricting glycolysis preserves T cell effector functions and augments checkpoint therapy. Cell Rep. *29*, 135–150.e9.

Schaefer, P.M., Hilpert, D., Niederschweiberer, M., Neuhauser, L., Kalinina, S., Calzia, E., Rueck, A., von Einem, B., and von Arnim, C.A.F. (2017). Mitochondrial matrix pH as a decisive factor in neurometabolic imaging. Neurophotonics *4*, 045004.

Scharping, N.E., Menk, A.V., Moreci, R.S., Whetstone, R.D., Dadey, R.E., Watkins, S.C., Ferris, R.L., and Delgoffe, G.M. (2016). The tumor microenvironment represses T cell mitochondrial biogenesis to drive intratumoral T cell metabolic insufficiency and dysfunction. Immunity *45*, 701–703.

Shivaswamy, V., Boerner, B., and Larsen, J. (2016). Post-transplant diabetes mellitus: causes, treatment, and impact on outcomes. Endocr. Rev. *37*, 37–61.

Su, X., Lu, W., and Rabinowitz, J.D. (2017). Metabolite spectral accuracy on orbitraps. Anal. Chem. *89*, 5940–5948.

Titov, D.V., Cracan, V., Goodman, R.P., Peng, J., Grabarek, Z., and Mootha, V.K. (2016). Complementation of mitochondrial electron transport chain by manipulation of the NAD+/NADH ratio. Science *352*, 231–235.

Vaeth, M., Maus, M., Klein-Hessling, S., Freinkman, E., Yang, J., Eckstein, M., Cameron, S., Turvey, S.E., Serfling, E., Berberich-Siebelt, F., et al. (2017). Store-operated Ca^{2+} entry controls clonal expansion of T cells through metabolic reprogramming. Immunity *47*, 664–679.e6.

van der Windt, G.J., and Pearce, E.L. (2012). Metabolic switching and fuel choice during T-cell differentiation and memory development. Immunol. Rev. *249*, 27–42.

Walenta, S., Salameh, A., Lyng, H., Evensen, J.F., Mitze, M., Rofstad, E.K., and Mueller-Klieser, W. (1997). Correlation of high lactate levels in head and neck tumors with incidence of metastasis. Am. J. Pathol. *150*, 409–415.

Walenta, S., Wetterling, M., Lehrke, M., Schwickert, G., Sundfør, K., Rofstad, E.K., and Mueller-Klieser, W. (2000). High lactate levels predict likelihood of metastases, tumor recurrence, and restricted patient survival in human cervical cancers. Cancer Res. *60*, 916–921.

Warburg, O., Posener, K., and Negelein, E. (1924). Über den stoffwechsel der tumoren. Biochem. Z. *152*, 319–344.

Xiao, H., Jiao, J., Wang, L., O'Brien, S., Newick, K., Wang, L.C., Falkensammer, E., Liu, Y., Han, R., Kapoor, V., et al. (2016). HDAC5 controls the functions of Foxp3(+) T-regulatory and CD8(+) T cells. Int. J. Cancer *138*, 2477–2486.

STAR★METHODS

KEY RESOURCES TABLE

REAGENT or RESOURCE	SOURCE	IDENTIFIER
Antibodies		
CD4 Monoclonal Antibody (GK1.5), Alexa Fluor 488	Thermo Fisher Scientific	Cat# 53-0041-82; RRID: AB_469893
CD4 Monoclonal Antibody (GK1.5), APC	Thermo Fisher Scientific	Cat# 17-0041-82; RRID: AB_469320
Rat Anti-CD4 Monoclonal Antibody, Pacific Blue Conjugated, Clone RM4-5	BD Biosciences	Cat# 558107; RRID: AB_397030
Rabbit Anti-beta-Actin Monoclonal Antibody, HRP Conjugated, Clone 13E5	Cell Signaling	Cat# 5125; RRID: AB_1903890
NFAT1 (D43B1) XP Rabbit mAb antibody	Cell Signaling	Cat# 5861; RRID: AB_10834808
Anti-NFAT1 (phospho S54) antibody (ab200819)	Abcam	Cat# ab200819
Dynabeads Mouse T-Activator CD3/CD28	Thermo Fisher Scientific	Cat# 11456D
Chemicals, Peptides, and Recombinant Proteins		
LIVE/DEAD Fixable Aqua Dead Cell Stain Kit	Thermo Fisher Scientific	Cat# L34966
CellTrace CFSE Cell Proliferation Kit	Thermo Fisher Scientific	Cat# C34554
Heptelidic Acid	Cayman Chemicals	Cat# 14079
Seahorse XF Cell Mito Stress Test Kit	Agilent	Cat# 103015-100
CD4+CD25+ Regulatory T Cell Isolation Kit, mouse	Miltenyi Biotec	Cat# 130-091-041
Sodium L-lactate	Millipore Sigma	Cat# L7022
Sodium D-lactate	Millipore Sigma	Cat# 71716
Sodium Pyruvate	Thermo Fischer Scientific	Cat# 11360070
Sodium Oxalate	Millipore Sigma	Cat# 223433
L-serine	Millipore Sigma	Cat# S4500
Cell-Tak	BD Biosciences	Cat# 354240
D-GLUCOSE (U-13C6, 99%)	Cambridge Isotope Laboratories	Cat# CLM-1396-PK
SODIUM PYRUVATE (13C3, 99%)	Cambridge Isotope Laboratories	Cat# CLM-2440-PK
SODIUM L-LACTATE (13C3, 98%)	Cambridge Isotope Laboratories	CLM-1579-PK
Calcium Sensor Dye eFluor 514	Thermo Fisher Scientific	Cat# 65085970
Bovine Serum Albumin Fraction V, heat shock, fatty acid free	Roche	Cat# 3117057001
Riboflavin 5-monophosphate sodium salt hydrate	Millipore Sigma	Cat# F6750
Resazurin sodium salt	Millipore Sigma	Cat# R7017
Diaphorase from *Clostridium kluyveri*	Millipore Sigma	Cat# D5540
Alcohol Dehydrogenase from *Saccharomyces cerevisiae*	Millipore Sigma	Cat# A3263
NAD	Roche	Cat# 10127965001
NADH	Roche	Cat# 10004634103
Critical Commercial Assays		
L-Lactate Assay Kit	Cayman Chemicals	Cat# 700510
iSTAT® $CG4^+$ cartridge	Abbott	Cat# 03P85-25
Experimental Models: Cell Lines		
C2C12 mouse myoblast cell line	American Type Culture Collection	ATCC Cat# CRL-1772, RRID:CVCL_0188
Ae17 mouse mesothelioma, sOVA	(Jackaman et al., 2003)	RRID:CVCL_LJ85

(*Continued on next page*)

Continued

REAGENT or RESOURCE	SOURCE	IDENTIFIER
Experimental Models: Organisms/Strains		
B6.129S7-*Rag1*^{tm1Mom}/J (B6/Rag1$^{-/-}$)	The Jackson Laboratory	Cat# JAX:002216, RRID:IMSR_JAX:002216
C57BL/6J	The Jackson Laboratory	Cat# JAX:000664, RRID:IMSR_JAX:000664
BALB/cJ	The Jackson Laboratory	Cat# JAX:000651, RRID:IMSR_JAX:000651
Software and Algorithms		
ImageJ64	NIH	https://imagej.nih.gov/ij/download
Wave 2.6.1	Agilent	https://www.agilent.com
Image Lab 5.2.1	Bio-Rad	https://www.bio-rad.com
Other		
RPMI 1640 Medium	Thermo Fisher Scientific	Cat# 11875085
Fetal Bovine Serum, certified, United States	Thermo Fisher Scientific	Cat# 16000044
RPMI 1640 medium, no glucose	Thermo Fisher Scientific	Cat# 11879020
Fetal Bovine Serum, dialyzed, US origin	Thermo Fisher Scientific	Cat# 26400044
Teknova RPMI-1640 Media without Glucose, Glycine and Serine	Teknova	Cat# 50-190-8105
DMEM, high glucose, GlutaMAX(™), pyruvate	Thermo Fisher Scientific	Cat# 10569
Seahorse XF Media & Calibrant	Agilent	Cat# 102353-100
CELLview culture dish	Greimer Bio-One	Cat# 627870
Microhematocrit Capillary Tubes, Heparinized	Thermo Fisher Scientific	Cat# 22-362-566

RESOURCE AVAILABILITY

Lead contact

Further information and requests for resources and reagents should be directed and will be fulfilled by the Lead Contact, Ulf H. Beier (beieru@email.chop.edu).

Materials availability

This study did not generate new unique reagents.

Data and code availability

This study did not generate any unique datasets or code.

EXPERIMENTAL MODEL AND SUBJECT DETAILS

Mice

We purchased B6/Rag1$^{-/-}$, C57BL/6J, and BALB/c mice from The Jackson Laboratory (Bar Harbor, ME). For most experiments, we used female 8-12 week old mice (elaborated in the method details below). Mice were housed under specific-pathogen-free conditions and studied using protocols approved by the Institutional Animal Care and Use Committees of the Children's Hospital of Philadelphia and the University of Pennsylvania (19-000561 and 20-000746).

Cell lines

C_2C_{12} cells, a spontaneously immortalized mouse myoblast cell line (CRL-1772; RRID:CVCL_0188), were obtained from American Type Culture Collection (ATCC); the C_2C_{12} cell line is female in origin. The Ae17 murine mesothelioma cell line was developed by injecting asbestos into the peritoneum of C57BL/6J mice and was transfected with secreted ovalbumin such that ovalbumin became a tumor marker. The cell line is female in origin (Jackaman et al., 2003).

Cell culture media and cell culture conditions

For standard cell culture medium, we used RPMI 1640 medium supplemented with 10% fetal bovine serum (FBS), penicillin (100 U × mL^{-1}), streptomycin (100 μg × mL^{-1}), and 55 nM β_2-mercaptoethanol. For low-glucose media, we used glucose-free RMPI-1640 (cat. #11879020) and FBS with glucose-free dialyzed FBS (cat. #26400036) from Thermo Fisher Scientific (Waltham, MA) and added

D-glucose as indicated. For serine-free media, we used RPMI 1640 without glucose, glycine, and serine, cat. #50-190-8105 (Teknova Inc, Hollister, CA), which was supplemented with sodium oxalate (cat. #223433, Sigma Aldrich), L-serine (cat. #S4500, Sigma Aldrich), and D-glucose as indicated. For cell culture of primary mouse fibroblasts and myoblasts, as well as C_2C_{12} cells, we used high glucose (25 mM), GlutaMAXTM, pyruvate Dulbecco's Modified Eagle's Medium (DMEM, cat. #10569, Thermo Fisher Scientific) with 20% FBS and added antibiotics as above. For bioenergetic measurements, we used Agilent Seahorse XF base medium (cat. #102353-100) from Agilent Technologies (Santa Clara, CA) plus 10 mM D-glucose, 1 mM Na pyruvate, and 2 mM L-glutamine 2 mM (without pyruvate/glucose for glycolytic stress test). Cells were cultured at 37°C with 5% CO_2, except for cells plated prior to Seahorse assays that require incubation without CO_2.

METHOD DETAILS

Bioenergetic measurements

We measured bioenergetic functions, OCR and ECAR using a XF24 and XF96 analyzer (Seahorse Biosciences, North Billerica, MA). For our T cells studies, XF24 or XF96 plates were coated using CellTak (BD Biosciences) as previously reported (Beier et al., 2015). C_2C_{12}, as well as primary mouse renal tubular epithelial, fibroblast, and mouse cells did not require CellTak. Isolated T cells were plated in unbuffered XF Assay Media, and then incubated for 30-60 min at 37°C without CO_2. For T cell studies, we used 1×10^6 cells per well for XF24, and 2×10^5 cells per well for XF96 assays. Primary mouse renal tubular epithelial cells were seeded at 8×10^4 cells per well, mouse primary fibroblasts and myoblasts at 4×10^4 cells per well, and C_2C_{12} cells at 2×10^4 cells per well (all in XF96 assays). To enhance cell adherence, plates were spun at room temperature for 5 min at 400 g. Three baseline measurements of OCR and ECAR were taken and then the cells were exposed to oligomycin A, cyanide-4-[trifluoromethoxy]phenylhydrazone (FCCP) and rotenone and/or antimycin A. For T cells and primary mouse renal tubular epithelial cells, we used 1.25 μM oligomycin, 0.5 μM FCCP and either 1 μM rotenone followed by 1.8 μM antimycin A in XF24, or 1 μM rotenone and antimycin A combined in XF96 experiments. For C_2C_{12} and primary mouse fibroblasts and myoblasts, we used 1 μM oligomycin, followed by two sequential 0.2 μM FCCP injections, and 1 μM antimycin A. Three readings were taken after each sequential injection. Instrumental background was measured in separate control wells using the same conditions without biological material. Seahorse reagents were purchased from Agilent Technologies (Wilmington, DE). Data were analyzed using Wave (Agilent), Excel and Prism.

Blood gas measurements

We obtained 70 μL of whole venous blood from mice via retroorbital blood collection as previously reported (Levine et al., 2016). Blood was collected in one heparinized Micro-Hematocrit capillary tube (Fisher Scientific, Cat. #: 22-362-566) per sample. Mice were anesthetized with isoflurane for each blood collection. The blood samples were then transferred onto an iSTAT® $CG4^+$ cartridge (Cat. #: 03P85-25, Abbott point of care Inc. Abbott Park, IL) utilizing an i-STAT 1 handheld analyzer (MN: 300-G, Abbott). Measured parameters (with detection ranges) included pH (6.5-8.2), pCO_2 (5-130 mmHg, 0.67-17.33 kPa), pO2 (5-800 mmHg, 0.7-106.6 kPa), and L-lactate (0.30-20.00 mM).

Cardiac allografting

For cardiac allografting, we transplanted BALB/c hearts (H-2^d) into the abdomen of C57BL/6J (H-2^b). We used female recipients and donors between 8-12 weeks of age, randomly assigned to treatment groups. We chose female mice to minimize fight injuries and ages 8-12 weeks to enable sufficiently large blood vessels to enable microsurgeries. Recipients received phenformin through intraperitoneal injection (70 mg × kg^{-1} × day^{-1}) for 14 days from engraftment. Allograft survival was assessed by daily palpation.

Cell isolation and flow cytometry

Spleen and peripheral lymph nodes were harvested and processed to single cell suspensions of lymphocytes. Red blood cells were removed with hypotonic lysis. We used magnetic beads (Miltenyi Biotec, San Diego, CA) for isolation of Tconv ($CD4^+CD25^-$) and Treg ($CD4^+CD25^+$). Cells of interest were analyzed flow cytometry. All flow cytometry data were captured using Cyan (Dako) as well as Cytoflex (Beckman Coulter, Brea, CA) and analyzed using FlowJo 10.2 software. For measurement of free intracellular calcium, we incubated T cells with eFlour™ 514 Calcium sensor dye (eBioscience) at 1 μM for 30 min at 37°C. We injected 1 μg × mL^{-1} ionomycin (Sigma) as a positive control. We used phosphate buffered saline with 2% FBS as flow buffer in all experiments except the calcium measurements under NAD^+:NADH polarizing conditions, where we added 30 mg × dL^{-1} D-glucose ± 20 mM NaCl, Na D-lactate or Na pyruvate, as NAD^+:NADH redox gradients disappear with cell washing and removal from polarizing environments.

Fluorescence Lifetime Imaging Microscopy (FLIM)

We isolated fresh murine $CD4^+CD25^-$ Tconv and placed them into a Cell-Tak-coated (BD Biosciences) four compartment CELLview cell culture dish with a thin glass bottom (cat. #627870, Greiner Bio-One, Kremsmünster, Austria), with 1×10^6 Tconv per compartment. Cells were exposed to 400 μL modified Tyrodes solution, containing 135 mM NaCl, 5 mM KCl, 1.8 mM $CaCl_2$, 20 mM HEPES (2-[4-(2-hydroxyethyl)piperazin-1-yl]ethanesulfonic acid), 5 mM D-glucose, 1 mM $MgCl_2$, and 1 mM L-glutamine. Tconv were stimulated with soluble anti-CD3ε and anti-CD28 mAb at 1 μg × mL^{-1} at the start of the experiment and allowed to incubate for 15 min in a

37°C heated microscope chamber at ambient CO_2. CD3ε/CD28 mAb beads and serum were avoided to minimize autofluorescence. NADH FLIM was performed as described (Schaefer et al., 2017). In brief, imaging was performed on a LSM 710 (Zeiss) and NADH was excited using a femtosecond-pulsed two-photon laser (Coherent). The NADH autofluorescence signal was detected through a 680 shortpass and 460/50 bandpass emission filter by time-correlated single photon counting (HPM-100-40 and SPCM 9.81, Becker and Hickl). FLIM images were analyzed by SPCImage 7.4 using a biexponential decay with T1 and T2 being variable using a binning of two. To avoid background, the minimum lifetime was set to 200 ps and a maximum Chi^2 of three was chosen. Five image sections were recorded per experiment each with displaying 20-40 Tconv. For "total," the average mean NADH lifetime of the whole image section was quantified. For mitochondrial and cytoplasmic/nuclear NADH, the phasor plot function of SPCImage 7.4 was used. The mitochondrial or cytoplasmic/nuclear phasors were selected by ROI, the decay curve summed up, shift was unfixed and then the mean NADH lifetime was quantified. To avoid any bias by cell or ROI selection, both FLIM measurements and analysis were blinded.

Glucose and L-lactate measurements

Glucose was measured by using a Contour® next EZ glucometer system (Bayer, Robinson Township, PA). We measured L-lactate through a fluorescence-based assay with recombinant LDH (Cayman Chemical, Ann Arbor, MI; cat. #700510) following the manufacturers' instructions. In the reaction, L-lactate is determined by the oxidation to pyruvate and the reduction of NAD^+ to NADH, with NADH binding to a fluorescent substrate. The samples were incubated for 20 min at room temperature and then measured with a Spectramax Gemini XPS plate reader using an excitation wavelength of 530-540 nm and reading an emission wavelength of 585-595 nm. Data were analyzed using SoftMax Pro 4.7 software (Molecular Devices, Sunnyvale, CA), MS Excel, and Prism.

Heavy carbon tracer labeling

Murine $CD4^+CD25^-$ Tconv cells were stimulated with CD3ε/CD28 mAb coated beads and 25 U × mL^{-1} IL-2 for 16 h. For labeling in Figure 1E, we added 20 mM [$^{13}C_3$] Na L-lactate (CLM-1579-PK, Cambridge Isotope Laboratories) to low-glucose media at 20 mg × dL^{-1} [$^{12}C_6$] D-glucose. For labeling in Figure 3, we used serine, glycine ,and glucose free media (cat. #R9660 Teknova Inc) supplemented with dialyzed FBS (cat. #26400036, Thermo Fisher Scientific) and added [$^{13}C_6$] D-glucose 60 mg × dL^{-1}. For Figure S3, we required media without background glucose and pyruvate. We used Seahorse XF DMEM medium (cat. #103575-100, Aligent) with dialyzed fetal bovine serum (FBS, cat. #26400036, Thermo Fisher Scientific). We added 10 mM $NaHCO_3$ as buffer as well as 6 mM L-glutamine. For labeling, we used 30-60 mg × dL^{-1} [$^{13}C_6$]-D-glucose (CLM-1396-PK from Cambridge Isotope Laboratories and cat. #389374, Millipore Sigma), and 1-41 mM [$^{13}C_3$] Na Pyruvate (CLM-2440-PK). Cells were exposed to labeling media for 3 h prior to harvest.

Immunoblotting

Purified stimulated Tconv were lysed in radioimmunoprecipitation assay (RIPA) buffer with Halt protease inhibitor (Thermo Fisher Scientific). Protein concentration was determined by photometry (DU640, Beckman-Coulter). Subsequently, samples were mixed with Laemmli sample buffer containing 2-mercaptoethanol (Bio-Rad Laboratories, Hercules, CA) and boiled for 5 min. The protein samples were loaded onto Mini-PROTEAN TGX™ 4 to 15% gradient gels (Bio-Rad) and underwent electrophoretic separation. Proteins were then transferred to PolyScreen PVDF Hybridization Transfer Membranes (PerkinElmer, Waltham, MA). Membranes were cut according to the molecular weights of the proteins of interest (as indicated with Precision Plus Protein Dual Color, Bio-Rad) and incubated with primary and horseradish peroxidase (HRP)–conjugated secondary antibodies. We used Super Signal West Pico chemiluminescent substrate (Thermo Fisher Scientific) and the ChemiDoc™ imaging system (Bio-Rad), using Image Lab™ software (Bio-Rad) for image file export. Images were processed with Adobe Photoshop Creative Cloud (auto contrast function).

Metabolite extraction and derivatization

Cells were harvested in 1 mL medium and washed with 10 mL ice cold Hanks' Balanced Salt Solution (ThermoFisher) with 8 mM D-glucose. Cells were quickly spun down (1,600 rpm, equivalent to 558.1 *g*, for 1 min, Heraeus X3R Multifuge, ThermoFisher), decanted and extracted with a –20°C pre-cooled mixture of methanol, acetonitrile, and water with 0.5% formic acid (all HPLC grade) at a ratio of 40:40:20, respectively. Extracted samples were vortexed, and 1.2 mL transferred to an Eppendorf tube and incubated on ice for 5 min. Samples were centrifuged (558.1 g, for 20 s) at 4°C, the supernatant neutralized with NH_4HCO_3 to pH 7 and immediately frozen at –80°C until analysis. For the assessment of glycolytic intermediates in activated Teff in the [^{13}C] carbon tracing experiments, rapid processing was essential. Here, we modified the extraction to process one sample at a time, which was rapidly spun in a 4°C pre-cooled centrifuge (Eppendorf 5415D at 13,200 rpm, equivalent to 14,227.2 *g*, for 20 s, including acceleration time). Subsequently, the sample was rapidly decanted and placed on dry ice. The cell pellet was then mixed and suspended in the above mentioned –20°C pre-cooled extraction buffer made of methanol, acetonitrile, and water with 0.5% formic acid (all HPLC grade) at a ratio of 40:40:20, respectively. The samples were subsequently centrifuged (Eppendorf 5415D at 13,200 rpm, equivalent to 14,227.2 *g*, for 20 s, including acceleration time), neutralized with NH_4HCO_3 to pH 7, and immediately frozen at –80°C until analysis.

NAD^+:NADH cycling assay

NAD^+ and NADH was measured using a modified enzymatic cycling assay based on Graeff and Lee (2002). Briefly, cells for NAD measurement were extracted with ice cold 0.6 M perchloric acid (Millipore Sigma), while cells for NADH measurement were extracted

using 0.25 M potassium hydroxide (Millipore Sigma) in 50% alcohol, centrifuged (Eppendorf 5417R at 14,000 rpm, equivalent to 18,188 *g*, for 10 min), and supernatants diluted 1:10 (NAD^+) or 1:5 (NADH) in 100 mM Na_2HPO_4 buffer, and pH adjusted to 8. Subsequently, 5 μL of extract or standard was added to 95 μL of cycling mix (0.1% Bovine serum albumin faction V, heat shock, fatty acid free (Roche, cat. #03117405001), 2% EtOH, 10 mM nicotinamide (Millipore Sigma, cat. #72345), 10 μM flavin mononucleotide (Sigma, cat. #F6750), 20 μM resazurin (Millipore Sigma, cat. #R7017), 10 μg × mL^{-1} diaphorase (Millipore Sigma, cat. #D5540), 100 μg × mL^{-1} alcohol dehydrogenase (Millipore Sigma, cat. #A3263) in 100 mM Na_2HPO_4 buffer, and pH adjusted to 8. The reaction fluorescence was read at emission of 590 nM with an excitation of 530/525 nM (Synergy H1, BioTek Winooski, VT). NAD and NADH standards serially diluted from stocks purchased from Roche (cat. #10127965001 and #10004634103, respectively).

Liquid chromatography mass spectrometry and reaction monitoring

Cell extracts were analyzed by liquid chromatography mass spectrometry (LC-MS) analysis on a Q Exactive PLUS hybrid quadrupole-orbitrap mass spectrometer (Thermo Scientific) coupled to hydrophilic interaction chromatography (HILIC) via electrospray ionization. The LC separation was performed on a XBridge BEH Amide column (150 mm × 2.1 mm, 2.5 μm particle size, Waters, Milford, MA) using a gradient of solvent A (95%:5% H_2O:acetonitrile with 20 mM ammonium acetate, 20 mM ammonium hydroxide, pH 9.4), and solvent B (100% acetonitrile). The gradient was 0 min, 85% B; 2 min, 85% B; 3 min, 80% B; 5 min, 80% B; 6 min, 75% B; 7 min, 75% B; 8 min, 70% B; 9 min, 70% B; 10 min, 50% B; 12 min, 50% B; 13 min, 25% B; 16 min, 25% B; 18 min, 0% B; 23 min, 0% B; 24 min, 85% B; 30 min, 85% B. The flow rate was 150 μL × min^{-1}. Injection volume was 10 μL and autosampler and column temperature were 4°C and 25°C, respectively. The MS scans were in negative ion mode with a resolution of 70,000 at m/z 200. The automatic gain control (AGC) target was 5 × 10^5 and the scan range was 75−1,000 at 1 Hz. Data were analyzed using MAVEN software (Melamud et al., 2010). Isotope labeling was corrected for natural abundance of [^{13}C] using an in-house correction code in R (Su et al., 2017). Data were exported using Thermo Xcalibur Qual Browser.

Tumor lactate measurements

Ova-expressing Ae17 lung mesothelioma (Jackaman et al., 2003) cells were grown in RPMI, 10% fetal bovine serum (FBS) supplemented with 2 mM L-glutamine. We injected 2 × 10^6 Ae17 tumor cells subcutaneously into the right flank of 6–8 week old female B6/Rag1$^{-/-}$ mice (female gender to avoid in-fighting). After six days, the mice were implanted an Alzet osmotic pump (filled with DMSO), which served as vehicle control during the evaluation of DMSO-soluble drugs and their effect on tumor size, and continued for an additional 7-10 days. Tumor volume was measured as previously reported (Xiao et al., 2016). The DMSO treated tumor samples were then harvested for lactate measurements. To avoid over-estimation of tumor lactate, the tumors were harvested within one min of euthanasia and immediately frozen in liquid nitrogen. As control tissue, we harvested liver tissue from the same mice after the tumor retrieval was completed (to avoid bias favoring higher lactate in tumors versus liver tissue). As an additional control, lung from healthy C67BL/6 mice was used. Liver and lung tissue were also frozen in liquid nitrogen, and, like the tumors, stored at –80°C. For tissue lactate extraction the samples were homogenized, thawed, and mixed 1:1 with 0.5 M metaphosphoric acid (HPO_3) to facilitate deproteinization (limiting artifacts from lactate production/consumption during sample preparation). Samples are then centrifuged at 10,000 *g* for 5 min at 4°C. Subsequently, the sample is neutralized by adding 2.2 μL $KHCO_3$, and then again centrifuged (10,000 *g*, 5 min, 4°C), and then diluted 1:1 with 50 mM K_2HPO_4, pH 7.5), and then underwent L-lactate measurements as described above.

QUANTIFICATION AND STATISTICAL ANALYSIS

Statistical analysis was performed using GraphPad Prism 8 software. Normally distributed data were displayed as means ± standard error of the mean (SEM) unless otherwise noted. Measurements between two groups were performed with an unpaired Student-t test if normally distributed, or Mann-Whitney U test if otherwise. For paired samples, we used a paired Student-t test or Wilcoxon matched-pairs signed rank test, depending on whether data were normally distributed, respectively. Groups of three or more were analyzed by one-way or two-way analysis of variance (ANOVA) or the Kruskal-Wallis test. Survival was assessed using Log-rank (Mantel-Cox) testing.